STABILITY INVESTIGATIONS OF AIRFOIL FLOW BY GLOBAL ANALYSIS

Marek Morzyński
Hermann Föttinger–Institut
Technische Universität, Berlin

Frank Thiele
Abteilung Turbulenzforschung
DLR, Berlin

Abstract

As the result of global, non-parallel flow stability analysis the single value of the disturbance growth-rate and respective frequency is obtained. This complex value characterizes the stability of the whole flow configuration and is not referred to any particular flow pattern. The global analysis assures that all the flow elements (wake, boundary and shear layer) are taken into account. The physical phenomena connected with the wake instability are properely reproduced by the global analysis. This enhance the investigations of instability of any 2-D flows, including ones in which the boundary layer instability effects are known to be of dominating importance. Assuming fully 2-D disturbance form, the global linear stability problem is formulated. The system of partial differential equations is solved for the eigenvalues and eigenvectors. The equations, written in the pure stream function formulation, are discretized via FDM using a curvilinear coordinate system. The complex eigenvalues and corresponding eigenvectors are evaluated by an iterative method. The investigations performed for various Reynolds numbers emphasise that the wake instability develops into the Karman vortex street. This phenomenon is shown to be connected with the first mode obtained from the non-parallel flow stability analysis. The higher modes are reflecting different physical phenomena as for example Tollmien-Schlichting waves, originating in the boundary layer and having the tendency to emerge as instabilities for the growing Reynolds number. The investigations are carried out for a circular cylinder, oblong ellipsis and airfoil. It is shown that the onset of the wake instability, the waves in the boundary layer, the shear layer instability are different solutions of the same eigenvalue problem, formulated using the non-parallel theory. The analysis offers large potential possibilities as the generalization of methods used till now for the stability analysis.

Introduction

The boundary layer stability analysis based on the solution of the Orr-Sommerfeld equation is a useful tool for practical analysis of the laminar-turbulent transition. The only competing method is based on purely empirical formulas, characterized most often by the shape parameter.

It is widely accepted that infinitely small disturbances, although amplified according to linear stability theory are not able to onset the laminar-turbulent transition unless the amplification reaches some value so a factor has to be introduced to correct the results of the analysis. The e^N method has been develop to match the results of the empirical an theoretical investigations.

The laminar-turbulent transition is usually preceded by the Tollmien-Schlichting waves. Several receptivity experiments (Morkovin [4]) were provided to understand the phenomena of the Tollmien-Schlichting waves generation. It is commonly accepted that Tollmien-Schlichting waves are generated by an external source of disturbance (as for example acoustic excitation) and that the non-parallel or non-uniform effects enhance the feedback between the wave and the excitation. These non-parallel and non-uniform effects are the viscous boundary layer growth, the change of the surface curvature and variation of the surface static pressure. The growth of the boundary layer is evident near the leading edge of the blunt body, change of the surface curvature causes the non-parallelity of the flow, surface static pressure changes significantly in the separation region. It is characteristic that these three problems were studied separately. Goldstein [1] solved analytically the problem of evolution of Tollmien-Schlichting waves near the leading edge. The influence of sudden change of the geometry was investigated by Goldstein [2] and Ruban [3] .

These investigations have one common feature - the assumption of slow variation of the flow in the streamwise direction as necessary condition for weakly non-parallel analysis.

Elliptic nature of the Navier-Stokes equation describing the flow suggest that the phenomena in all these regions are not independent and influence each other. The question arises if interactions of the leading edge geometry, boundary layer and wake can be described by a single theory. The natural choice is to drop the parallel flow assumption and to treat the flow in all these regions as a whole. The consequence is the attempt to use the non-parallel flow, global stability analysis. The non-parallel theory was succesfuly used to study the wake instability [10, 9, 8, 7, 12]. There are no theoretical limitations to apply this analysis also to various geometries, as for example the airfoil. Because the assumptions of the non-parallel theory is a generalization of the classical parallel flow analysis, one can expect that this method is adequate not only for determination of the wake instability. The instability of the boundary and shear layer must be reflected in the eigenvalue solutions of the problem.

Governing equations

Linear stability theory is concerned with the development in time and space of infinitesimal perturbations around a given basic flow. If this basic flow is assumed to be parallel, the classical theory of parallel shear flow stability can be applied. This method has been also successfully used for nearly parallel flows for which the multiple-scale method, adopting the concept of "slow" variation of flow parameters in one direction, is valid. In general, non-parallel case only the two-dimensional theory taking into account the non-parallel effects is adequate. The equations of this theory are briefly presented here.

The problem was solved in the pure (Lagrangian) stream function finite difference formulation. This formulation, not

very common in the Navier-Stokes equations solvers, offers certain advantages for the eigenvalue analysis. The primitive variables formulation ([9]) results in much larger matrices. Although the eigenvalues are equal for velocities and pressure one has to deal with the full system. This difference in size is even more evident because the matrix entries are complex for the eigenvalue analysis.

The unsteady incompressible Navier-Stokes equations written in the stream function formulation take the form:

$$\Big[\frac{\partial}{\partial t} + (\nabla \times \vec{\psi}) \cdot \nabla - \frac{1}{Re}\Delta\Big]\Delta\vec{\psi} = 0 \qquad (1)$$

$$\vec{\psi} = \psi \vec{e_3} \qquad (2)$$

We assume that the stream function $\vec{\psi}(x,y,t)$ is a sum of a steady part $\bar{\psi}(x,y)$ and the unsteady disturbance $\vec{\psi}'(x,y,t)$:

$$\vec{\psi}(x,y,t) = \bar{\psi}(x,y) + \vec{\psi}'(x,y,t) \qquad (3)$$

The disturbance value is assumed to be small compared to the stream function value. Introducing equation (3) into (1) we obtain the nonlinear equation:

$$\Big[\frac{\partial}{\partial t}+(\nabla\times\bar{\psi})\cdot\nabla-\frac{1}{Re}\Delta\Big]\Delta\vec{\psi}'+(\nabla\times\vec{\psi}')\cdot\nabla(\Delta\bar{\psi}+\Delta\vec{\psi}') = 0 \quad (4)$$

Assuming a small disturbance allows the linearization of the equation (4) i.e. we ignore the terms containing $(\vec{\psi}')^2$. In the disturbance equation we separate the time and space dependence:

$$\vec{\psi}'(x,y,t) = \vec{\varphi}(x,y)e^{-i\lambda t} \qquad (5)$$

where

$$\lambda = \pi(St + i\sigma) \qquad (6)$$

Introducing the above relationship into (4) results in the linear partial differential equation:

$$i\lambda\Delta\vec{\varphi} - (\nabla\times\bar{\psi})\cdot\nabla\Delta\vec{\varphi} - (\nabla\times\vec{\varphi})\cdot\nabla\Delta\bar{\psi} + \frac{1}{Re}\Delta^2\vec{\varphi} = 0 \quad (7)$$

The fundamental difference between this equation and the Orr-Sommerfeld one, which is derived in similar manner assuming the disturbance form as:

$$\vec{\psi}'(x,y,t) = \vec{\varphi}(y)e^{i(\alpha x-\beta t)} \qquad (8)$$

is that, while Orr-Sommerfeld equation is an ordinary differential equation, equation (5) is a partial differential equation. This means different methods of solution and numerical problems encountered for the two cases.

To solve the problem for an arbitrary flow geometry the curvilinear body fitted coordinate system should be used for the solution of the equation (1) and (7). For orthogonal metric the following relations are valid:

$$g_{ij} = 0 \quad , \quad g^{ij} = 0 \quad , \quad i \neq j \qquad (9)$$

hence equations (1) and (7) can be written as:

$$g^{ii}\Big[\frac{\partial}{\partial t}\psi\Big|_{ii} + e^{mn3}\psi\Big|_n\psi\Big|_{iim} - \frac{1}{Re}g^{jj}\psi\Big|_{iijj}\Big] = 0 \qquad (10)$$

$$g^{ii}\Big[i\lambda\psi\Big|_{ii} - e^{mn3}(\psi\Big|_n\varphi\Big|_{iim} + \varphi\Big|_n\psi\Big|_{iim} + \frac{1}{Re}g^{jj}\psi\Big|_{iijj}\Big] = 0 \quad (11)$$

The symbol $\big|$ denotes the covariant derivative of the function. For further specialized metric tensor coefficients

$$\begin{aligned} g_{11} &= \alpha^2(\xi)g(\xi,\eta) \\ g_{22} &= \beta^2(\eta)g(\xi,\eta) \end{aligned} \qquad (12)$$

only $g(\xi,\eta)$ and its first order derivatives $g_{,\xi}$ and $g_{,\eta}$ have to be calculated for any transformation.

Reynolds number Re and Strouhal number St are expressed as:

$$Re := \frac{dU_\infty}{\nu} \quad ; \quad St := \frac{df}{U_\infty} \qquad (13)$$

Discretized, equation (11) can be written as:

$$(A - \lambda B)\varphi = 0 \qquad (14)$$

and represents the generalized eigenvalue problem.
For the eigenvalue calculations complex numbers can be split into real and imaginary parts so that only the real arithmetic has to be applied. Then the two parts of equation (2.10) may be written:

$$\begin{aligned} A\varphi_r - \lambda_r B\varphi_r + \lambda_i B\varphi_i = 0 \\ A\varphi_i - \lambda_i B\varphi_r + \lambda_r B\varphi_i = 0 \end{aligned} \qquad (15)$$

Solution

Numerical discretization and meshes

The discretization of the Navier-Stokes equations (11) and disturbance equation (12) is accomplished using the finite difference method. In both cases the thirteen-point stencil was used. The accuracy of the derivatives for such a stencil is maximum $0(h^2)$ for the fourth order terms.The unsteady version contains implicit stepping in time.

For all the calculations the orthogonal O-type mesh obtained by the conformal mapping is applied. The Karman-Trefftz transformation was used for the airfoil calculations. The metric coefficients (13) are expressed analytically by means of symbolic manipulation program to assure the maximum accuracy.

Boundary Conditions

For the steady Navier-Stokes equation solution the following boundary conditions are used:

$$\psi = 0 \quad , \quad \psi_{,n} = 0 \quad \textit{on the body} \qquad (16)$$

$$\frac{D\omega}{Dt} = 0 \quad , \quad \psi_{,n} = \psi_{pot,n} \quad \textit{in the farfield} \qquad (17)$$

The collocation of the vorticity transport equation is made only for the outflow. For the inflow the Dirichlet boundary condition with the value of the potential flow solution is taken. The boundary conditions for the disturbance equation (12) are:

$$\varphi = 0 \quad , \quad \varphi_{,n} = 0 \quad \textit{on the body} \qquad (18)$$

$$\frac{D\omega}{Dt} = 0 \quad , \quad \frac{D\varphi}{Dt} = 0 \quad \textit{in the farfield} \qquad (19)$$

The Dirichlet boundary condition (zero disturbance) is introduced for the inflow. The introduction of the convective boundary conditions appears to be an important factor of improving the numerical accuracy, especially for the steady and unsteady flow calculations.

Solution of the eigenvalue problem

In any eigenvalue problem the question arises whether all the eigenvalues are sought or whether determination of only one or few is satisfactory. Solving similar problem Zebib and Kim et al. [10,11] applied the QZ type decomposition from the standard libraries. The advantage of finding all of the eigenvalues is that no guess values have to be made. For relatively small matrix size, resulting from the use of the spectral method or crude FDM meshes this procedure is acceptable and was used in our earlier investigations [7]. Jackson applied for the unsymmetrical, complex generalized eigenvalue problem, appearing in the non-parallel flow stability theory the inverse iteration method [9]. This concept is also adopted in our present investigations. The eigenvalue, closest to the guess value and the related eigenvector are both determined at the same time. Till now it is the only realistic method for very large equation systems.

The following equations explain the principle steps of this method. Applying the Newton-Raphson method to equation (14) we obtain

$$(A - \lambda^{(n)}B)(\varphi^{(n)} + d\varphi^{(n)}) - d\lambda^{(n)}B\varphi^{(n)} = 0 \qquad (20)$$

which can be written as:

$$(A - \lambda^{(n)}B)\eta^{(n+1)} = B\varphi^{(n)} \qquad (21)$$

where the normalization is performed as follows:

$$\varphi^{(n+1)} = \varphi^{(n)} + d\varphi^{(n)} \qquad (22)$$

and

$$(e^r)_i = \delta_{ir} \qquad (23)$$

denotes a unit vector. The correction of $d\lambda^{(n)}$ is calculated from:

$$d\lambda^{(n+1)} = \frac{1}{(e^r)^T\eta^{(n+1)}} \qquad (24)$$

The iteration process involves the repeated solution of the equation (21), normalization of the eigenvector and correction of the eigenvalue. This process continues until convergence of the eigenvector and eigenvalue is achieved. The procedure, which consists of LU decomposition at each step with a quadratic rate of convergence, was replaced by a method using only one LU decomposition. The convergence is then only linear but the back-substitution time is significantly reduced compared to the decomposition time, justifying many iteration steps:

$$(A - \lambda_o B)^{-1}B\varphi^{(n)} = \eta^{(n+1)} \qquad (25)$$

The scheme is found to be convergent to the eigenvalue closest to λ_o and to produce the appropriate eigenvector.

Numerical results

The linear stability analysis consist of two steps. First the steady solution of the Navier-Stokes equations has to be found. In practice both, the steady and unsteady solution of the Navier-Stokes equations was performed. The unsteady one served as the reference data for the comparison to the results of eigenvalue analysis. It is characteristic that obtaining of the unsteady solution near the critical Reynolds number is difficult. For symmetrical flow some external forcing has to be introduced. The response of the flow field is dependent on the way the disturbance is introduced. The nearly neutral stability of the flow caused that the influence of the disturbance dominates the flow even after a long time. In this case the purely numerical aspects of the computation are of much greater significance. Also unsymmetrical flows near the critical Reynolds number requires a lot of CPU time to become fully unstable. The flow patterns of initial periods are different from the "fully developed" unsteady ones (Fig.12). Near the critical Reynolds number such patterns can persist over a long time requiring significant amount of CPU time to obtain the real periodic state. Some codes fail to carry out the calculations long enough in time and due to unphysical boundary conditions the solution breaks down when the vorticity reaches the outflow boundary. The unsteady simulation for the Reynolds number higher than the critical one is easier. For this reason always the higher Reynolds number unsteady solutions were taken for the comparison with the stability analysis.

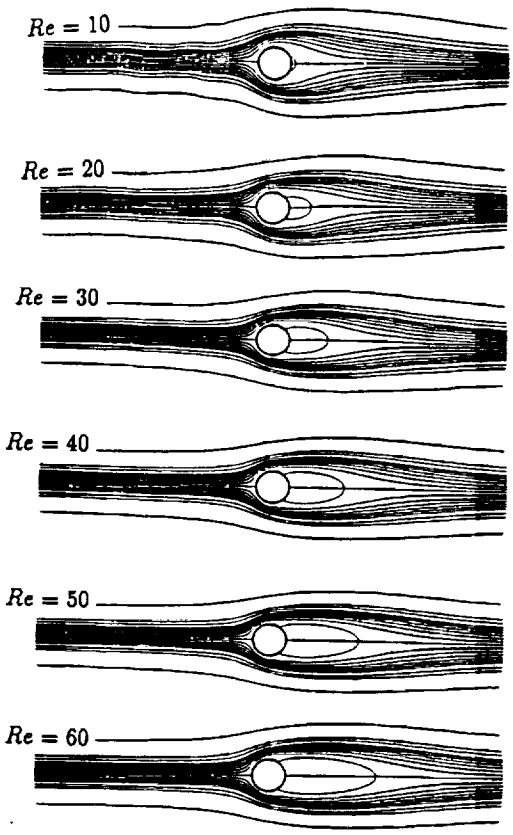

Figure 1: Steady flow solutions for the circular cylinder flow

In the linear stability theory the Navier-Stokes equations are linearized about a steady flow. The quality of the steady solution has then the direct influence on the eigenvalue analysis. The accuracy of the solution is the best for the circular cylinder flow and is decreasing for the ellipsis

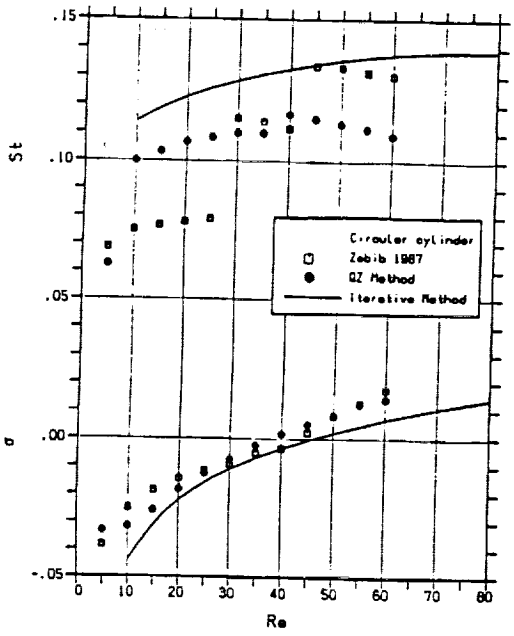

Figure 2: The growth-rate and the Strouhal number for the circular cylinder flow.

and airfoil flow where leading and trailing edge can cause numerical problems even for meshes generated by the conformal mapping. In case of limited computer resources it is satisfactory for the numerical simulation of the flow to use relatively crude mesh spacing on central, upper and lower parts of the airfoil. In this case the gradients of the quantities along the boundary layer are not very large. For the eigenvalue analysis however, also the fine discretization in this direction is very important. The attempt to detect the Tollmien-Schlichting waves necessities at least several tenth of points for one period preserving also the fine discretization in the radial direction. The compromise for these two contradictory requirements was partly obtained by calculation of the steady solution on one mesh and interpolation of the result on another mesh, more suitable for the stability calculations.

The eigenvalue solution was calculated for the external flow around the circular cylinder, ellipsis and an airfoil. The circular cylinder served as the source of reference data, for the validation of the program because a lot of numerical and experimental results is avaiable. The only existing results for non-parallel analysis are the circular cylinder results [10, 9]. The flow around the ellipsis was investigated to analyze different eigenmodes. The modes characterized by higher frequency are clearly appearing for high Reynolds numbers. Because of the extremely long wake for $Re > 200$, causing several numerical difficulties such an analysis could not be carried out for the circular cylinder. Finally the NACA 4412 airfoil flow for $\alpha = 0^0$ and $\alpha = 15^0$ was shown to examine the potential possibilities connected with the eigenvalue analysis of this geometry.

Circular cylinder results

For the symmetrical flow around cylinders it is always,

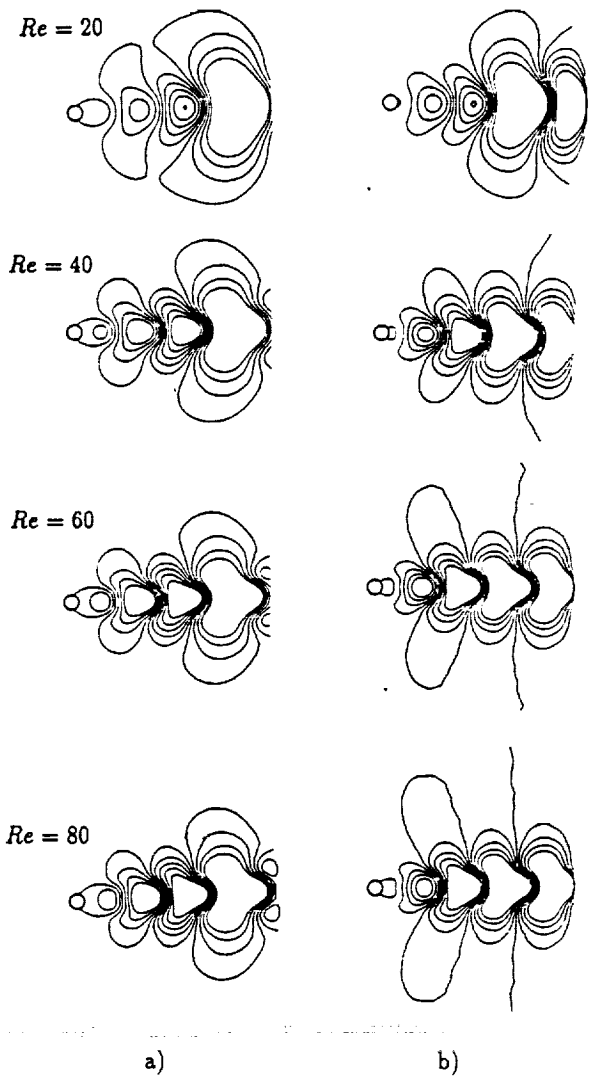

Figure 3: Real (a) and imaginary (b) part of the eigenvector.

theoretically, possible to obtain a steady-state solution, even above the critical Reynolds number. The streamlines patterns obtained for the steady flow around a circular cylinder are shown in Fig.1. These results served as the input data for the eigenvalue analysis. The guess value for the Strouhal number is 0.12 and the growth-rate 0. The result of the calculation consist of the complex eigenvalue for each Reynolds number together with a complex eigenvector. The growth-rate and the corresponding frequency as the function of the Reynolds number is shown in Fig.2. Some results of our previous investigations using the QZ method are also plotted. The results of these calculations are compared with those obtained by Zebib [10], which uses the non-parallel analysis in the spectral stream function formulation together with a full-matrix eigenvalue solver of a QZ-type. For the inverse iteration method, used in our computations, the critical values are $Re_c = 46.23$ and $St_c = 0.1345$.

The real and imaginary part of an eigenvector for the increasing Reynolds number is depicted in Fig.3. Over a wide

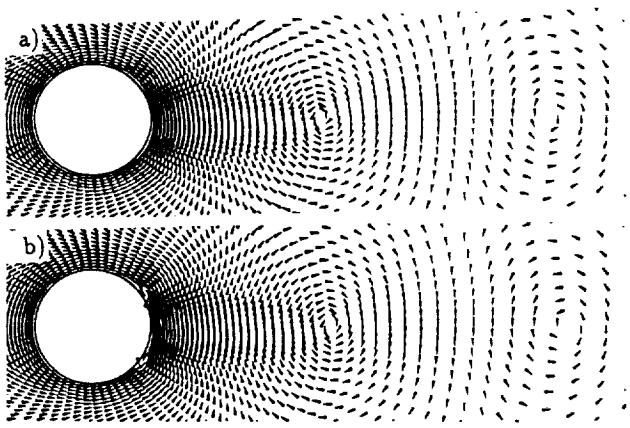

Figure 4: Eigenvector velocities (imaginary part): (a) below Re_c ($Re = 40$) (b) above Re_c ($Re = 50$).

range of Reynolds numbers the eigenvector (disturbance) patterns are very similar, showing the physical aspects of the phenomena to be already present in flows of fairly small Reynolds number. The increase in Reynolds number allows these modes to cross the zero-growth-rate line and emerge as instabilities. The problem arises if there is any difference in eigenvector patterns bellow and above the critical Reynolds number. It is known from the parallel flow stability analysis that the wake stability is governed by its characteristics in the vicinity of the rear stagnation point. Careful study of the eigenvector values near the cylinder shows (Fig.4) the difference in the disturbance patterns above the Re_c. This enhance the onset of the Karman vortex street.

To evaluate how realistic are the obtained eigenvalue solutions the disturbance is summed with the steady-state solution for $Re = 90$. As the reference the unsteady flow simulation for Re=100 is taken (Fig.5). The same periodic patterns are present in both pictures. This proves that for the cylinder flow instability the non-linear effects are not significant.

Ellipsis flow

Following the approach for the circular cylinder flow the elliptic cylinder was analyzed. It is known from experiments and non-parallel flow stability analysis of Jackson, performed for the bodies with different cross-sections that the proper scaling of Strouhal number is based on the dimension perpendicular to the main flow direction. For such a scaling its value is not much different for various shape of the cylinder. The critical Reynolds number reflects also the overall shape of the body. The relation between the axis ratio of the ellipsis and the critical Reynolds number was studied earlier [8]. For the oblong ellipsis situated parallel to the flow direction the critical Reynolds number is increasing while the slope of the growth-rate curve becomes smaller, comparing to the circular cylinder results. As can be expected the Karman vortex street mode results differ only slightly from ones obtained for the circular cylinder. The eigenvector patterns, growth-rate and frequency relations for increasing Reynolds numbers are similar to the circular cylinder ones. The interesting results are obtained also for the Reynolds number higher than the critical one. We assume that the steady flow solution coincides with the real one in the boundary layer and

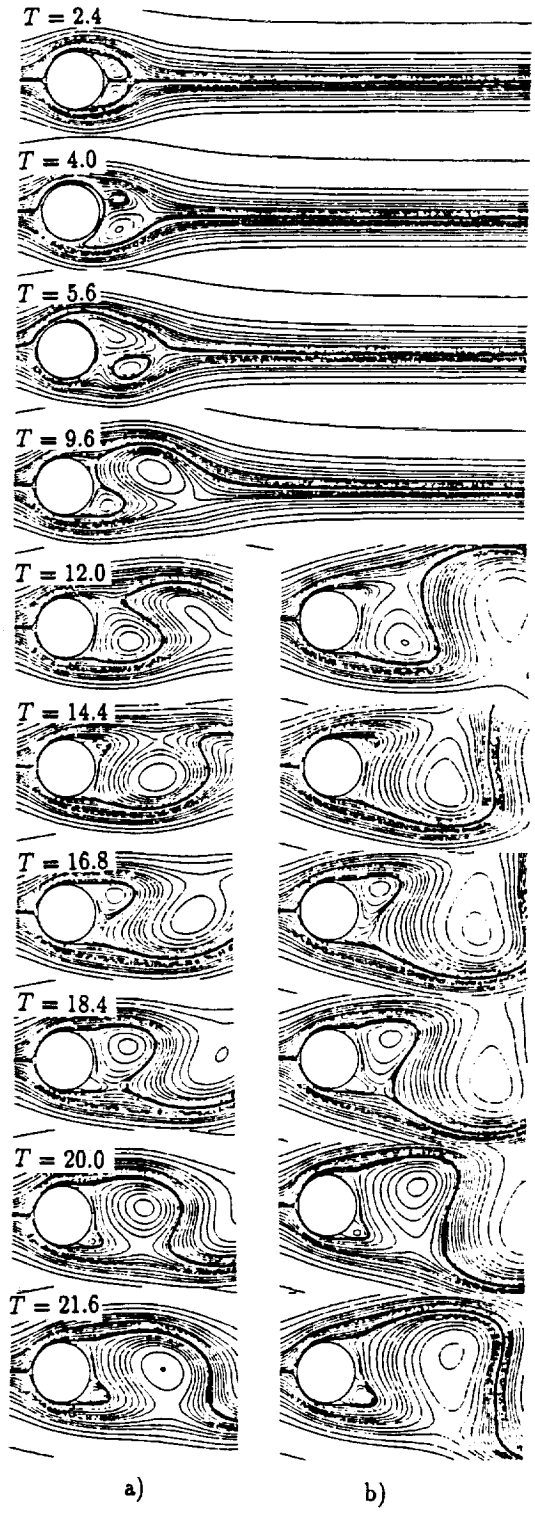

Figure 5: Karman vortex street (a) superposition of the disturbance and steady solution, $Re = 90$ (b) unsteady simulation, $Re = 100$

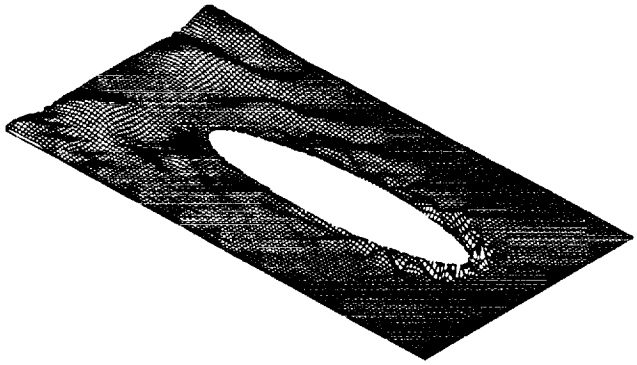

Figure 6: Higher mode eigenvector (real part) for the 1:5 ellipsis flow, $Re = 200$

the shear layer near the body, even for the Reynolds number higher than the critical one. The justification for such an assumption are the experimental investigations of Kourta et al. [13] and Unal and Rockwell [14] in the higher Reynolds number range the Karman vortices are formed not directly behind the cylinder. Between the cylinder and the vortex street a dead fluid zone is found, bounded by two nearly parallel shear layers. As the Reynolds number increases the length of the dead-fluid zone decreases and the location of the first instability waves in the shear layer moves upstream. According to the results of the parallel flow stability analysis the unsteady behavior of the fluid is governed by the flow in direct neighborhood of the body. This conclusion allows us to cut the steady solution and limit the computational domain. The fact that the length of the wake, obtained as the steady-state solution of the Navier-Stokes equations exceeds the assumed "infinity" distance (the wake end is outside the computational domain) is in context of the eigenvalue analysis not relevant.

This steady flow solution is was used as the base for the eigenvalue analysis. The assumed guess frequency is higher than for the Karman vortex mode. The result of the higher mode analysis is depicted in Fig.7 and 8. The growth-rate is a function of both Reynolds number and mode, so that different modes are preferentially amplified as the Reynolds number increases. In Fig. 7 the growth-rate and the Strouhal number for higher mode is depicted together with the first one for the ellipsis having the axis ratio 1:5. The temporal evolution of the waves is shown in Fig. 8. The amplitude of the wave is raising in the direction of the separation. The waves on the upper and lower surface of the ellipsis are shifted in phase as the result of superposition of the symmetric pattern of disturbances and antisymmetric stream function. The characteristic patterns for all higher modes investigated are the family of branches of disturbance streamlines having sequentially positive and negative values. Each branch is ended with a cell located in the vicinity of the maximum velocity gradients in the boundary or shear layer. The eigenvector patterns should be analyzed in connection with the steady flow solution. The disturbance is added to it to obtain the unsteady flow. In the steady solution two regions can be distinguished - "soft" part where the stream function

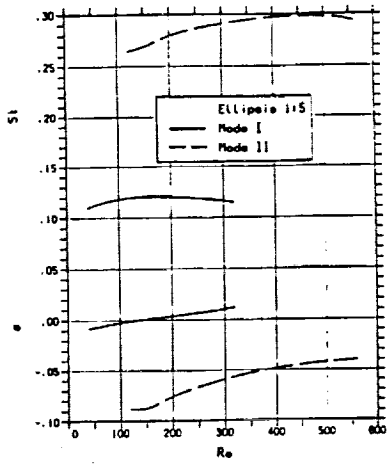

Figure 7: The growth-rate and the Strouhal number for the for 1:5 ellipsis flow

values are small, containing the boundary layer, separation and wake region and the "stiff" part where the stream function values are large in comparison to the disturbance. It is obvious that when adding the disturbance and steady state solution only the "soft" part is "modulated" while the "stiff" one is practically not influenced (Fig.8). For this reason the considerations concerning the eigenvector patterns outside the "soft" region have very limited practical meaning. This conclusion is confirmed by numerical calculations, showing that the "soft" regions of the eigenvector are related to the growth-rate and frequency value. The rest of the field is more likely influenced by numerical aspects of the computations.

For the Blasius profile instability the Tollmien-Schlichting wave length is approximately six times larger than the boundary layer thickness. Since the boundary layer on the ellipsis is relatively thick for the range of the Reynolds numbers applied in the calculations the detected Tollmien-Schlichting waves are also long. The shorter ones, for higher Reynolds numbers require much finer meshes, especially in the circumferential direction. The eigenvector cells, located on the ellipsis surface near the leading edge are shorter (in the circumferential direction) than the ones in the separation region. For a given constant frequency which is the same for the whole field it can mean only that the wave propagates slower near the leading edge and faster in the separation region. The propagation along the shear layer of the wake has approximately constant velocity. All the found eigenvalues for the Tollmien-Schlichting mode were damped ones. The question arises if the Tollmien-Schlichting wave, considered globally, in the boundary layer and propagating further along shear layer can become amplified without external excitation. The growth-rate is raising with the increasing Reynolds number and one can expect that the higher mode wave will become only slightly damped or even amplified for the high enough Reynolds number.

For any flow around the cylinder exist many eigenmodes. In practice near any given frequency exist an eigenvalue, mostly with such an low growth-rate that it is unlikely that

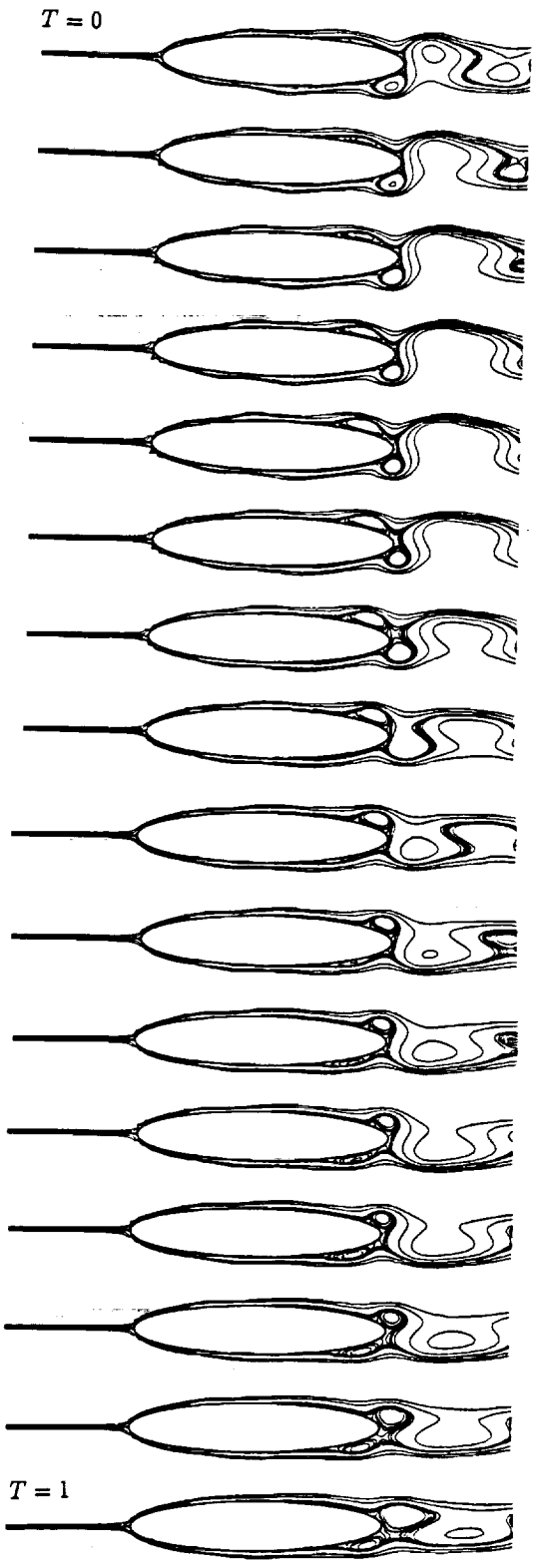

Figure 8: Tollmien-Schlichting waves - temporal evolution for the 1:5 ellipsis flow, $Re = 200$

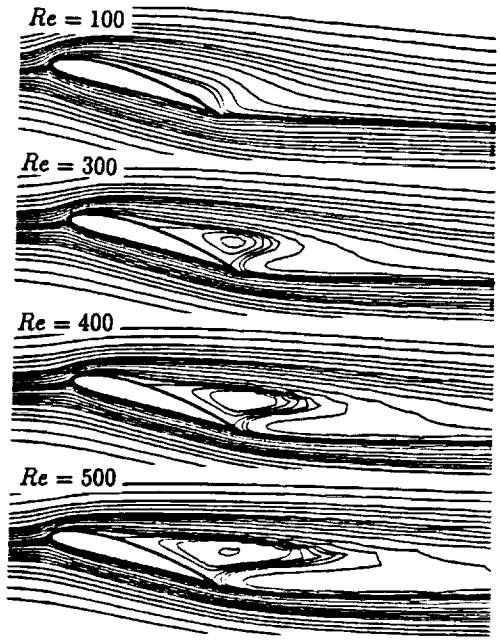

Figure 9: Steady flow solutions - NACA 4412, $\alpha = 15^0$

it can emerge as the instability. Similar conclusions can be drawn on base of the Kim [11] results.

Different eigenvectors can be classified into at least two groups. One characteristic eigenvector pattern is connected with the onset of the Karman vortex street. Fig.3 shows this mode for the circular cylinder. Jackson [9] has shown the same patterns. Similar mode was detected by Karniadakis et al. [5] who investigated the flow around the circular cylinder placed in the channel bounded with two parallel plates. This mode is called there the central mode and dominates for the cylinder placed near the symmetry axis. Moving the cylinder toward the wall causes switching to the "wall mode" which is related to the Tollmien-Schlichting waves. For the external flow around the cylinder the "wall" mode forms similar cells located however on the body and in the shear layer.

The airfoil flow

The another cylinder flow which was considered is the airfoil flow. As the example geometry the NACA4412 airfoil is taken. Two different angles of attack were considered. For $\alpha = 15^0$ the stall is evident and the regular Karman vortex street appears for high enough Reynolds number. The numerical simulation of such a flow was performed by Shütz [6]. For $\alpha = 0^0$ dominating phenomena take place in the boundary and shear layer.

First the steady flow solution has been found (Fig.9). The character of the steady flow solution for $\alpha = 15^0$ is different from the circular cylinder one. (Fig.1, Fig.9). While for the circular cylinder the wake consist ot two bubles, there is only one for the airfoil flow.

The eigenvalue analysis gave the fastest growing mode (Fig.10).

For $\alpha = 15^0$ the flow becomes unstable at $Re = 335$. The eigenvector patterns are in this case also very similar to ones for the circular cylinder (Fig.11). In Fig.13 the comparison

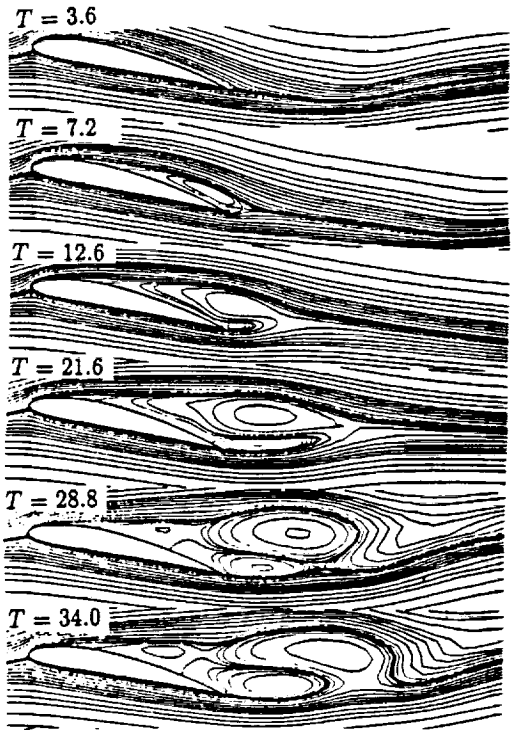

Figure 12: Early time steps, NACA 4412 flow, $Re = 1000$, unsteady simulation

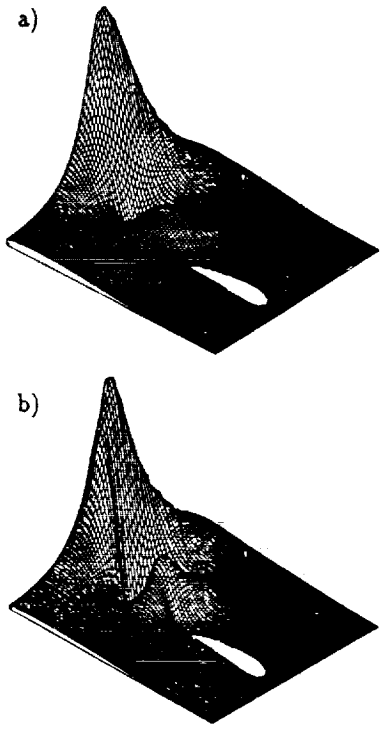

Figure 13: Real part of the eigenvector - airfoil flow, $\alpha = 15^0$ a) $Re = 100$, b) $Re = 600$

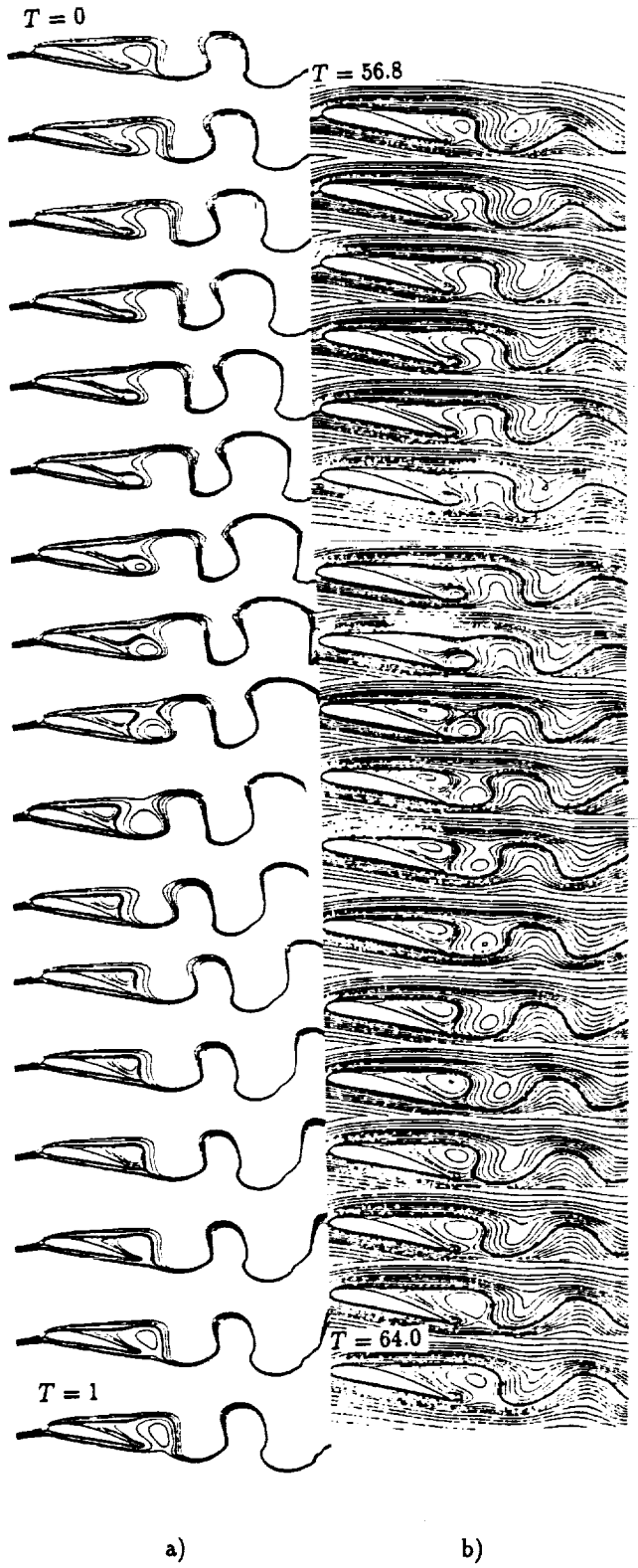

Figure 14: NACA 4412 airfoil flow: (a) superposition of the steady solution and disturbance fields, $Re = 600$, (b) unsteady simulation, $Re = 1000$

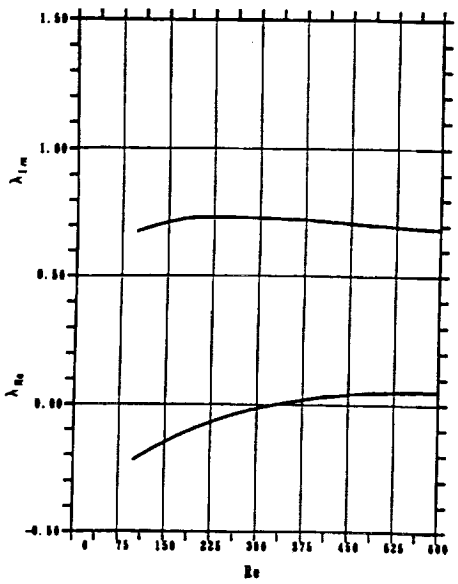

Figure 10: The growth-rate and the Strouhal number for the airfoil flow

between the real part of the eigenvector for $Re = 100$ and $Re = 500$ is shown. The value of the disturbance is growing with the flow direction for both cases. It is normalized, so the disturbance reaches the same maximum, located in the vicinity of the outflow boundary. Because for $Re = 100$ (Fig.13) the growth-rate is negative the disturbance will be damped after a long enough time. The flow for $Re = 500$ is unstable. The disturbance is growing both in time and in the flow direction. The characteristic feature for the higher Reynolds numbers flows is the much larger amplitudes of the disturbance in the wake close to the airfoil.

To compare the obtained eigenvalue analysis results with the real flow patterns the unsteady simulation was used. The simulation was performed for $Re = 1000$. The early stages of unsteady simulation exhibit patterns significantly different from the "fully developed" ones (Fig.12). This discrepancy is even greater in the neighborhood of the critical value. For this reason to compare with the eigenvalue analysis one period was taken after long enough time ($t = 56.8$ to $t = 64.0$). Earlier periods are "spoiled" by the initial flow development. The comparison of the flow patterns for $Re = 600$ (eigenvalue analysis) and $Re = 1000$ (unsteady simulation) show very good qualitative agreement. All the mechanisms of the vortex shedding are properly reproduced. This fact is one more proof that the Karman vortex street, especially near the body has the linear character.

For the angle of attack equal 0^0 till $Re = 800$ exists no separation on the airfoil. The higher mode solution forms two row of cells (Fig.15) which are close to the airfoil only near the leading edge. When added to the steady flow solution only the shear layer behind the airfoil is effected (Fig.16). The flow is stable because the growth-rate is negative, but if it becomes unstable it is the Kelvin-Helmholz type of instability of the shear layer. For increasing Reynolds numbers the cells

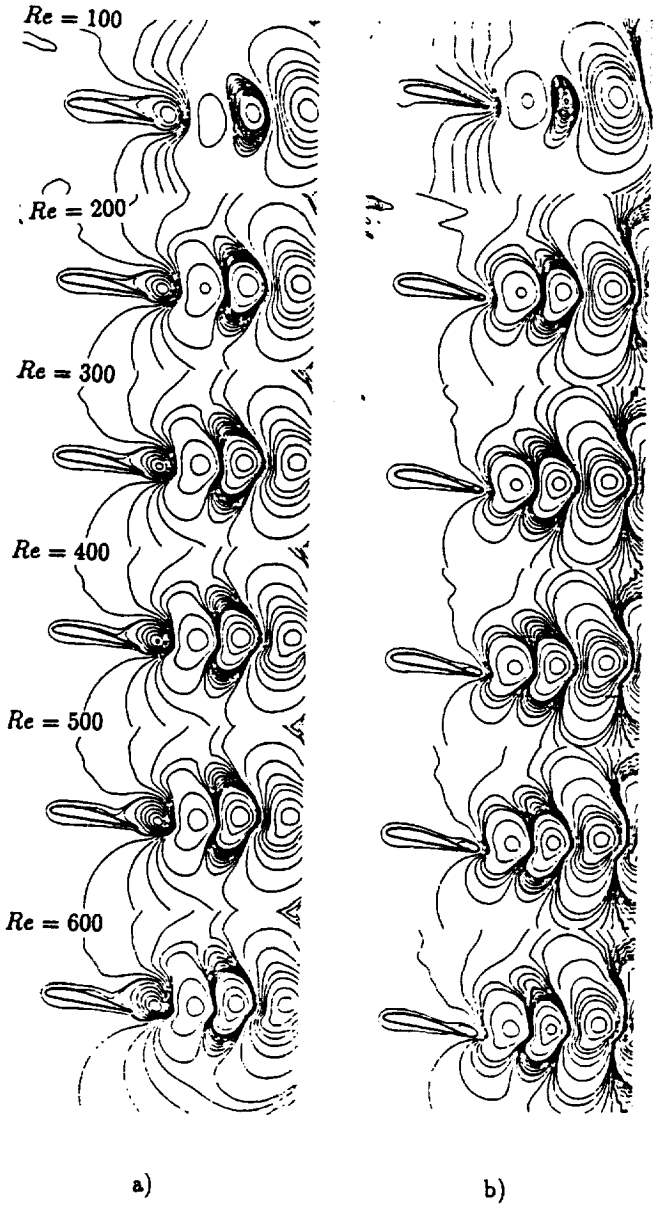

Figure 11: Real (a) and imaginary (b) part of the eigenvector - airfoil flow, $\alpha = 15^0$

are moving closer to the airfoil. The disturbances form now cells attaching the airfoil and forming the "wall" mode. The boundary layer is now "modulated" in the way simlar to the ellipsis flow. For $\alpha = 0^0$ the Karman vortex street mode also exists, although it is strongly damped for the small Reynolds numbers.

Conclusions

It was shown that non-parallel flow stability analysis is a method most suitable for determination of the wake flow instability. Several examples , calculated for different Reynolds numbers and geometries ranging from circular cylinder to the airfoil with the angle of attack, show that the method is a general tool for prediction of the wake instability. It is of advantage of this method, comparing to other numerical ap-

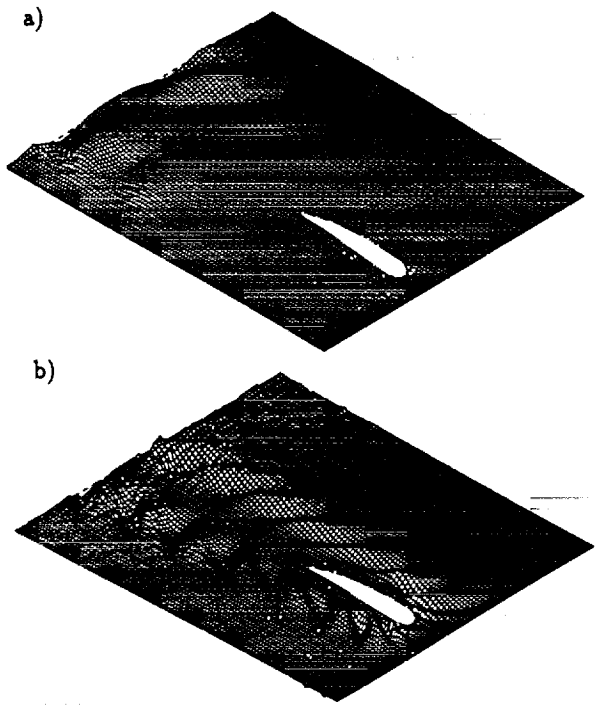

Figure 15: Higher mode solution for the NACA 4412 airfoil $\alpha = 0^0$, a) $Re = 300$, b) $Re = 900$

Figure 16: Superposition of the steady solution and higher mode disturbance for the NACA 4412 airfoil, $Re = 300$

proaches, that the critical Reynolds numbers and respective frequencies are determined more precisely. The method is able to handle the unsymmetrical wake flow. In this calculations the superiority of the stream function formulation and iterative determination of the eigenvalue has been proved.

Using the same method higher modes were investigated for the ellipsis and airfoil flow. Although the investigations had a preliminary character it can be concluded, that the results obtained differ significantly from the first mode solution. The higher mode disturbance patterns, obtained for the ellipsis flow, added to the steady solution appear to be the Tollmien-Schlichting wave originating in the boundary layer. The wave propagates further along the mixing layer. For the airfoil flow these types of modes were found but also another instability phenomena are present in the eigenvalue solutions. The investigation of large spectrum of eigenmodes is even more difficult because some instability phenomena are smoothly "switching" to another ones. The result of the higher-mode analysis gives the qualitative insight into the stability problem. The limitation of the method on present state of its development is not the formulation but the numerical approach. These difficulties we hope to overcome in our future investigations.

We belive that the method presented here will enable the stability analysis of any flow as a whole, without breaking it into pieces or restricting considerations to single type and that all instability phenomena are reflected in the non-parallel flow eigenvalue solutions.

References

[1] M.E.Goldstein, The evolution of Tollmien-Schlichting waves near a leading edge, J. Fluid Mech. 127, (1983), 59-81.

[2] M.E.Goldstein, Scattering of acoustic waves into Tollmien-Schlichting waves by small streamwise variations in surface geometry , J. Fluid Mech. 154, (1985), 509-529.

[3] A.I.Ruban, On the generation of Tollmien-Schlichting waves by sound, Fluid Dyn. 19, (1985), 709-716.

[4] M.V.Morkovin, Critical evaluation of transition from laminar to turbulent shear layers with emphasis on hypersonically traveling bodies, AFFDL-TR-68-149, (1969).

[5] G.E.Karniadakis, B.B.Mikic, A.T.Patera, Minimum-dissipation transport enhancment by flow destabilization: Reynolds' analogy revisited, J. Fluid Mech. 192, (1988), 365-391.

[6] H.Schütz, Ein direktes Lösungsverfahren der Navier-Stokes Gleichungen in reiner Stromfunktionsformulierung zur Simulation instationärer inkompressibler Strömungen in zweidimensionalen Geometrien, Doktor Dissertation, Berlin 1990.

[7] D.Wolter, M.Morzynski, H.Schütz, F.Thiele, Numerische Untersuchungen zur Stabilität der Kreiszylinderströmung, Z. angew. Math. Mech., 69, (1989), 6, 601-604.

[8] M. Morzyński, F.Thiele, Numerical stability analysis of a flow about a cylinder, Z. angew. Math. Mech., 71, (1991), 5, T424-T428.

[9] C.P.Jackson, A Finite-Element study of the onset of vortex shedding in flow past variously shaped bodies, J. Fluid Mech. 182, (1987), 23-45.

[10] A.Zebib, Stability of viscous flow past a circular cylinder, J. of Eng. Math., 21, (1987), 155-165.

[11] I.Kim, A.J.Pearlstein, Stability of the flow past a sphere, J. Fluid Mech. 211, (1990), 73-93.

[12] M. Morzyński, F.Thiele, Non-parallel stability analysis of wake and boundary layer flow, Boundary Layer Control Conference, Cambridge, 9-12 April 1991, 15.1-15.11.

[13] A.Kourta, H.C.Boisson, P.Chassaing, H.Ha Minh, Nonlinear interaction and transition to turbulence in the wake of a circular cylinder, J. Fluid Mech. 181, (1987), 141-161

[14] M.F.Unal, D.Rockwell, On vortex formation from a cylinder. Part 1. The initial instability. Part 2. Control by splitter-plate interference. J. Fluid Mech., 190, (1988), 491-529